29 May 2010, 8:00 am - 9:30 am

Shaking Table Methodology and Instrumentation for Reinforced Soil Retaining Walls

Saman Zarnani
GeoEngineering Centre at Queen's-RMC, Kingston, Canada

Richard J. Bathurst
GeoEngineering Centre at Queen's-RMC, Kingston, Canada

W. Andy Take
GeoEngineering Centre at Queen's-RMC, Kingston, Canada


Fifth International Conference on
Recent Advances in Geotechnical Earthquake Engineering and Soil Dynamics
and Symposium in Honor of Professor I.M. Idriss
May 24-29, 2010 • San Diego, California

SHAKING TABLE METHODOLOGY AND INSTRUMENTATION FOR REINFORCED SOIL RETAINING WALLS

Saman Zarnani
GeoEngineering Centre at Queen's-RMC
Kingston, Ontario
K7L 3N6, Canada

Richard J. Bathurst
GeoEngineering Centre at Queen's-RMC
Kingston, Ontario
K7L 3N6, Canada

W. Andy Take
GeoEngineering Centre at Queen's-RMC
Kingston, Ontario
K7L 3N6, Canada

ABSTRACT

The paper describes a testing methodology, instrumentation array and example data interpretation for reduced-scale geosynthetic reinforced soil (GRS) wall models built on a large shaking table. The testing program is unique in the literature because of the large number of different instruments deployed and the use of Particle Image Velocimetry (PIV) analysis of imagery captured using a high speed camera. The models are instrumented with strain gauges and extensometers attached to the geogrid reinforcing layers, LVDTs attached to the facing panel, load cells at the wall toe, reinforcement-facing load measurement, and accelerometers in the backfill and along the facing. Example measurements are reported that demonstrate the value of the experimental technique to better understand the mechanics of these systems under simulated earthquake.

INTRODUCTION

The superior seismic performance of relatively ductile geosynthetic reinforced soil (GRS) retaining walls has been demonstrated by comparison to the poor performance of relatively rigid conventional gravity-type retaining walls subjected to the same earthquake event (Collin et al. 1992; Sandri 1997; White and Holtz 1997; Tatsuoka et al. 1995, 1997a,b; Ling et al. 2001; Bathurst et al. 2002; Koseki et al. 2006). Nevertheless, there are deficiencies in the current design of these systems and fundamental lack of understanding of the mechanics of these complex systems during earthquake loading. Current seismic design of these systems is based on pseudo-static methods, which are largely extensions of Coulomb wedge methods (Mononobe-Okabe (M-O) theory), or the Newmark sliding block concept (Bathurst et al. 2002). The accuracy of these approaches has not been adequately validated against measured physical data which is most commonly gathered from shaking table testing. Furthermore, results of numerical simulations have illustrated that the magnitude and distribution of reinforcement loads during seismic loading are different from predictions using pseudo-static methods (Bathurst and Hatami 1998).

Shaking table experiments on reduced-scale models are the most practical approach to gain further qualitative and quantitative understanding of the behavior of GRS walls under seismic loading. A disadvantage of a reduced-scale test is that the response of the model may differ from prototype-scale systems due to low confining pressure (i.e. stress-level dependent properties of granular backfills), far-end boundary conditions and improperly scaled mechanical properties of the soil reinforcement materials. Nevertheless, qualitative insights are possible using this experimental approach. Furthermore, the models can be used to validate the accuracy of numerical codes and analytical methods that can be used in turn to investigate wall response at prototype scale.

Most experimental tests on seismic behavior of GRS walls have been performed on very small-scale models where scale effects are expected to have a major influence on measured response. Some examples include: Lo Grasso et al. (2004), H (model wall height) = 0.35 m; Watanabe et al. (2003), Kato et al. (2002) and Koseki et al. (1998), H = 0.5 m. There are also some seismic tests on larger models: El Emam and Bathurst (2004), Matsuo et al. (1998), Bathurst et al. (1996), H = 1 m; Sakaguchi (1996), H = 1.5 m and Ling et al. (2005), H = 2.8 m.

This paper presents details of large shaking table-GRS model wall test design, instrumentation and monitoring developed at the Royal Military College of Canada (RMC) and some example test results. The example model wall described here is 1.42 m in height and is one of a series of experiments that are underway to investigate seismic performance of GRS walls.

EXPERIMENTAL SET UP

General Arrangement

A new shaking table facility has been recently commissioned at RMC. The table is comprised of a steel platform with plan dimensions of 2.6 m by 3.3 m and is driven by a 250 kN capacity actuator with maximum horizontal acceleration of 1g at ±125 mm stroke with full payload. Excitation is in the horizontal direction (one degree of freedom only). The platform is seated on a pair of very low friction linear bearings (rails) mounted in turn on a pair of heavily reinforced concrete footings. The actuator is computer-controlled and can be driven using simple excitation records or actual earthquake (horizontal) accelerograms. A rigid steel "strong box" is rigidly connected to the steel platform and is used to contain the backfill soil and GRS model. The box sidewalls and back wall are comprised of rigid steel sections supporting transparent 25 mm-thick Plexiglas sheets. One end of the box is open to provide access to the GRS wall models. The box is 1.5 m high by 2.28 m wide (width of the GRS model wall) and 2.56 m long (the depth of the backfill soil behind the wall). Two layers of transparent polyethylene sheet were used to cover the inside of the Plexiglas in order to minimize side wall friction and thus approach as far as practical an idealized plane strain condition. Layers of plywood were fixed to the steel platform and a thin layer of sand was glued to the top sheet to create a rough interface at the bottom of the backfill soil. The far-end boundary of the model walls is also rigid which can be expected to influence the dynamic response of the GRS model wall due to reflected energy as demonstrated numerically by Bathurst and Hatami (1998). However, this boundary condition is unavoidable in physical experiments of this type but can be explicitly accounted for in numerical simulations used to verify computer models and these verified numerical models used to investigate other boundary conditions.

Figure 1 illustrates a cross section of the shaking table platform, strong box, wall facing and instrumentation. The GRS wall was built as a rigid propped panel wall. The facing consisted of twenty stacked 64 × 64 mm hollow steel sections bolted together (section mass = 5.82 kg/m). The height and length of wall facing panel was 1.45 m and 2.27 m, respectively. The cross section dimensions of the facing panel sections and weight (and hence inertia) were selected to satisfy dynamic physical model scaling laws proposed by Iai (1989) assuming a model to prototype scaling factor of 1/4. Each end of the facing panels was slotted and bolted between two vertical steel angles (Fig. 2).

In previous numerical (Bathurst and Hatami 1998) and experimental studies (El Emam and Bathurst 2005) it has been shown that the toe restraint condition at the wall footing has a significant effect on wall displacements, distribution and magnitude of reinforcement loads, and the overall performance of GRS walls during simulated earthquake loading. For the example shaking table test in this paper, a hinged footing condition was selected (i.e. toe restrained in the vertical and horizontal directions while free to rotate about the base) (Fig. 3). The facing panel was seated on a steel base plate which in turn was supported by four linear bearings

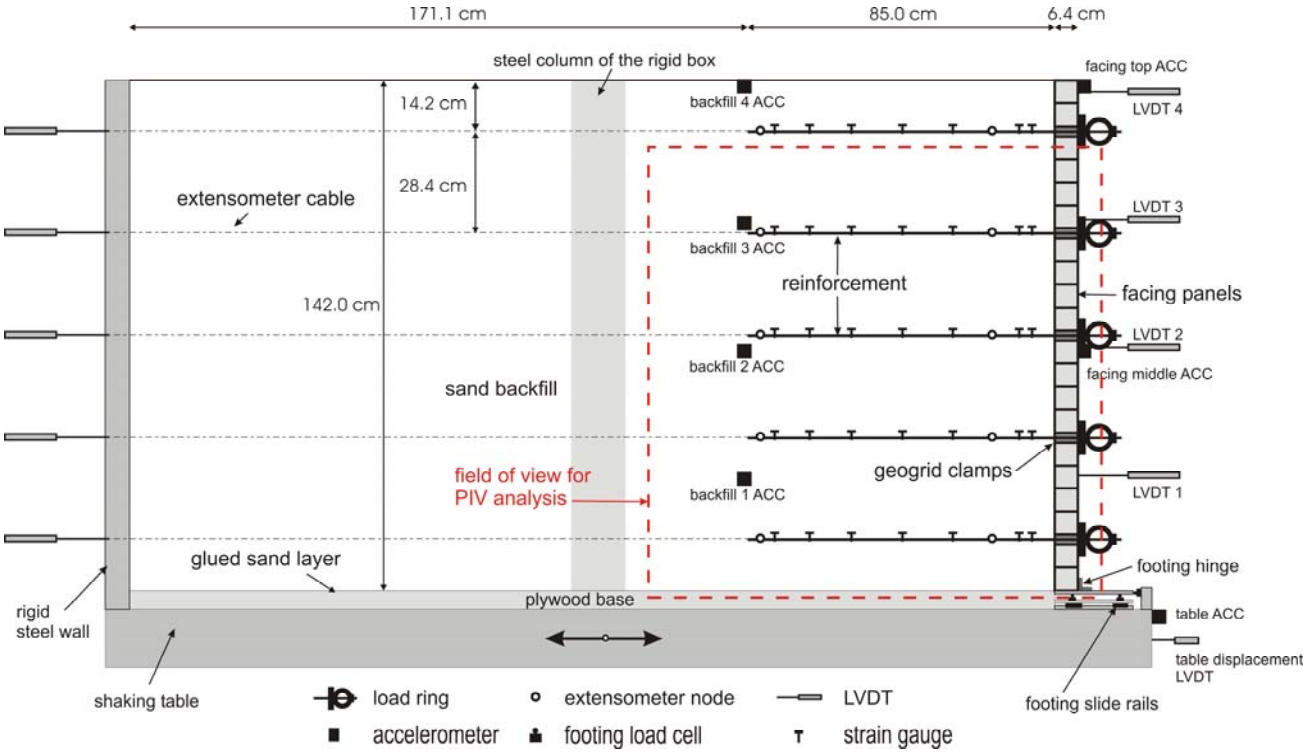

Fig. 1. Cross section of the model GRS wall

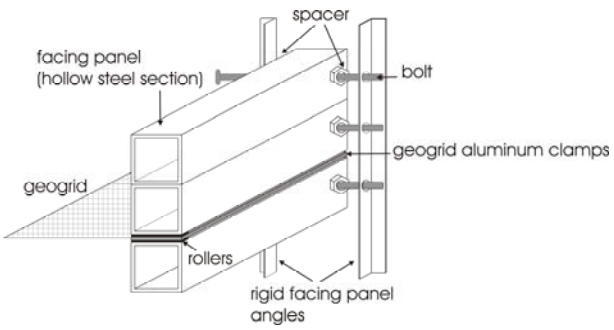

Fig. 2. Rigid panel facing detail

(slide rails) bolted to the shaking table platform. Thus friction at the toe in the horizontal direction was effectively eliminated and the horizontal and vertical forces measured at the toe are fully decoupled. The footing boundary condition in this test can be considered to be one of two limiting cases with respect to actual field structures. The other idealized footing condition is a horizontally unrestrained toe which can be created by removing the horizontal load cell mounted against the footing base plate. The advantage of measuring decoupled boundary forces at the toe is that these values can be used to validate predicted boundary loads using numerical models.

The length of the geogrid reinforcement layer was L = 0.85 m giving L/H = 0.6. This low value of L/H matches the minimum value recommended by the National Concrete Masonry Association (NCMA 1998) for the design of segmental (modular block) retaining walls.

During construction of the model wall, two vertical supports were placed in front of the wall in order to brace the facing and prevent it from moving during construction. The loose sand backfill was placed in 150 mm-lifts. The shaking table was excited at 6 Hz after each lift in order to vibro-compact the backfill sand. At the end of construction the two facing supports were released and the wall was allowed to reach static equilibrium. This stage was taken as datum for most subsequent dynamic measurements.

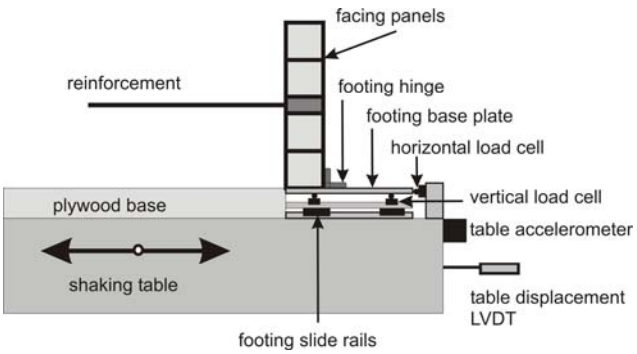

Fig. 3. Footing detail

Instrumentation

Figure 1 illustrates the instrumentation adopted for this shaking table experimental program. The acceleration and horizontal displacement of the shaking table was monitored with an accelerometer and a LVDT attached to the table platform. The displacements of the facing panel were monitored using four LVDTs placed against the wall face. Two accelerometers were attached to the facing panel at mid-height and top of the wall to measure the acceleration response of the facing. Four other accelerometers were placed inside the backfill soil at equal vertical spacing and about 0.9 m from the wall. The capacity of accelerometers was either ±2g or ±5g. The higher capacity accelerometers were placed at higher elevations along the facing panel and in the backfill soil where greater accelerations were anticipated. Each backfill accelerometer was placed within a small volume of soil contained within a thin-walled plastic ring 75 mm in diameter and 50 mm high. This technique was used to ensure that the accelerometer was in phase with the backfill soil during shaking.

The decoupled horizontal and vertical toe loads were measured with two horizontal load cells and eight vertical load cells (Fig. 3). Geogrid layer responses were monitored by eight pairs of strain gauges glued to the longitudinal members of the geogrid. The Wheatstone Bridge circuitry adopted for each (top and bottom) pair of gauges resulted in cancellation of bending strains and hence only local axial strains in the geogrid were recorded. Two pairs of strain gauges were attached to the geogrid immediately adjacent to the facing panel. The average global movement (or strain) in each reinforcement layer was monitored by two LVDTs located at the back of the strong box and connected to monitoring points on the geogrid with extensometer wires. The accelerometers in the backfill and along the facing, LVDT extensometers, facing LVDTs and reinforcement strain gauges were located over the middle width of the model to further minimize potential side wall boundary effects. A row of load rings was used to measure tensile loads at each of the geogrid-facing connections. A novel mechanical arrangement was developed to improve the measurement of tensile connection loads (Fig. 4). The geogrid layer was clamped between two aluminum flat bars with the same width as the facing panels and the bars screwed together tightly. Six small rollers were placed below and above the aluminum clamp so that the entire tensile

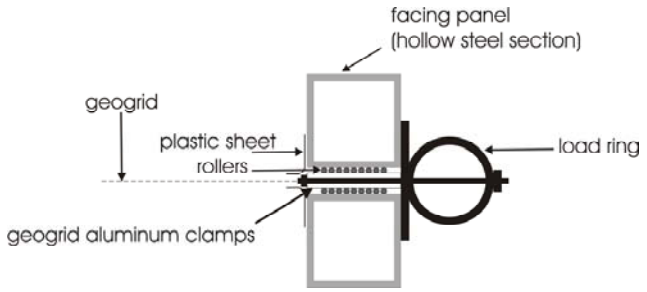

Fig. 4. Connection load ring attachment detail

connection load is transferred to the connection load rings. The spacers placed between the facing panel and the vertical angles (Fig. 2) allow the geogrid clamping arrangement to perform without interference from the vertical angles placed at the two ends of the facing panel.

All the instruments were connected to a high speed synchronous data acquisition system. The data was acquired at the rate of 200 Hz in order to prevent any aliasing effects.

To the best knowledge of the writers, non-contact method Particle Image Velocimetry (PIV) was used for the first time to measure wall model response This technique involves analyzing sequential digital images and measuring the displacement of pixel patches between them (White et al. 2003). These digital images capture the arrangement of soil particles in an image matrix that contains the intensity (brightness) recorded at each pixel using a CCD (Charged Coupled Device) camera.

For this shaking table test a high speed digital video camera with 1600 × 1200 pixel resolution was used. The frame rate was restricted to100 Hz due to hard drive capacity of the video camera. With this resolution and frame rate, about 30 seconds of video could be captured by the camera. The camera field of view is shown in Fig. 1. In order to capture this field of view the camera had to be located 5 m from the side of the shaking table. The video was shot through the transparent Plexiglas/polyethylene side walls of the shaking table strong box. For PIV analysis, the video was converted into digital still images. A matrix of 199 patches with the size of 50 × 50 pixels was then generated to cover the field of view for PIV analysis. PIV analysis was carried out using code written for Matlab software and the movement of each patch was calculated for each image. At the focal length used to capture these images, the size of a pixel corresponds to 1.196 mm in object space. Thus the tracked patches correspond to backfill soil regions of about 60 × 60 mm. The precision of PIV analysis is about $1/10^{th}$ of a pixel (White et al. 2003) or about 0.1 mm in this test.

Input Excitation

After initial static equilibrium was achieved in the model, a variable-amplitude harmonic excitation was used as the input base excitation to shake the model. This accelerogram has both increasing and decaying peak acceleration portions and is expressed as:

$$\ddot{u}(t) = \sqrt{\beta e^{-\alpha t} t^{\zeta}} \sin(2\pi f t) \quad (1)$$

In this non-dimensional equation β, α and ζ are user-defined variables, t is time in seconds, and f is the desired frequency in Hz (5 Hz in this example). The accelerogram generated by this equation does not require any base line correction. The displacement record was calculated by double integration and was applied to the shaking table using the computer-controlled actuator. The final input acceleration was applied to the model wall in eight stages of the reference accelerogram with increasing acceleration amplitude at each stage. Hence, the first stage had maximum acceleration amplitude of about 0.1g and the last stage had maximum acceleration amplitude of about 0.55g. Figure 5 shows the measured shaking table acceleration during the first stage. After each stage there was a pause of seven minutes during which the video file captured during each stage was downloaded for PIV analysis. There was no detectable influence of the pause between excitation stages on the collected data.

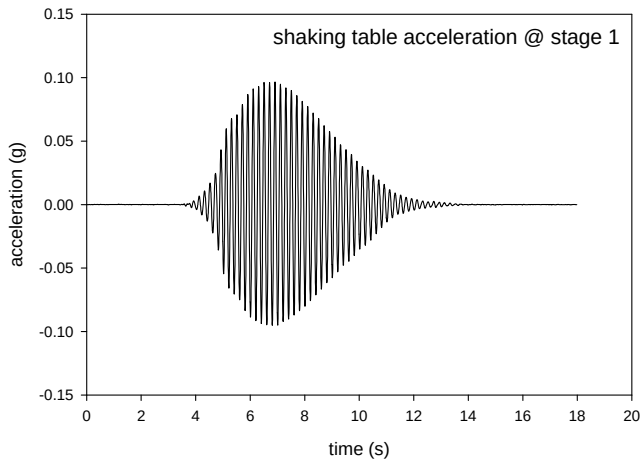

Fig. 5. Measured shaking table acceleration during stage 1 of shaking

MATERIAL PROPERTIES

The backfill soil was clean, uniform-sized, rounded beach sand (SP in the Unified Soil Classification System) with D_{50} = 0.357 mm, coefficient of curvature, C_c = 2.27 and coefficient of uniformity, C_u = 1.09. The fines content (particle sizes < 0.075 mm) was about 1%. This sand has a constant volume friction angle of 35° and a peak plane strain friction angle of 44° (Bathurst et al. 2001; Hatami and Bathurst 2005). The sand has an almost flat compaction curve which helped to ensure that the final compacted density was uniform through the entire backfill. The dry density and the moisture content of the backfill soil was measured with a nuclear density meter after each lift of sand was vibro-compacted and leveled. The average dry density and moisture content of the compacted backfill were 1700 ± 50 kg/m^3 and 1.3 ± 0.5%, respectively. Based on the compaction curve for this sand, the dry density is equivalent to about 96% of Modified Proctor compaction.

Numerical studies (Rowe and Hoe 1998; Bathurst and Hatami 1998; Hatami et al. 2001) and field measurements (Allen and Bathurst 2002) have shown that reinforcement stiffness (rather than tensile strength at rupture) is a key parameter influencing tensile loads in reinforcement layers under operational conditions. Hence, proper scaling of the reinforcement material is important but often ignored in reduced-scale

physical modeling of GRS walls. The scaling laws proposed by Iai (1989) were used in this research program to select a commercially available knitted polyester (PET) geogrid that had suitable reinforcement stiffness. This geogrid has a thin polyvinyl chloride (PVC) coating and an aperture size of 23 mm by 24 mm. The width of the strands in the cross-machine direction was greater than in the machine direction which made these strands more suitable for attaching strain gauges. Hence, the geogrid was placed with the cross-machine direction in the direction of loading. The tensile strength of this geogrid was determined by performing in-air single strand tensile tests at a rate of 10%/min on 300 mm-long cross-machine strands. The tensile strength was 4.3 kN/m at 2% strain and 5.8 kN/m at 5% strain. The stiffness of this geogrid material (J_m at 2% strain) was computed to be J_m = 215 kN/m (reduced-scale model with height = 1.42 m). This model geogrid is equivalent to a geogrid with a stiffness at prototype scale (wall height assumed as 6 m) $J_p = J_m \times \lambda^2$ = 3793 kN/m, where λ = 6 m/1.42 m = 4.2). This value is typical for geogrid products used in field walls.

MEASUREMENT RESULTS

In this section some typical measurement results are presented to illustrate the type and quality of data that was gathered during the example shaking table test.

Facing LVDTs

Figure 6 illustrates (typical) facing horizontal movement measured at facing LVDT 3 over the entire shaking program. The measurements show increasing permanent facing horizontal movement after each shaking stage of 20 seconds duration. Figure 7 illustrates the maximum accumulated facing horizontal movement profile at each stage measured by the four LVDTs mounted against the facing. At the last stage the top of the facing panel had moved about 190 mm. The plotted facing profiles show that up to stage 6 the facing panel behaved as a rigid panel as originally intended but during the last two stages the space between some stacked facing units opened up resulting in the appearance of local bending of the facing.

Accelerometers

Figure 8 shows the maximum measured accelerations recorded by all accelerometers attached to the shaking table, facing panel and embedded in the backfill soil. The results show that as the base input acceleration increased at each stage, the acceleration response measured by other accelerometers also increased but with amplified magnitude. The exception to this

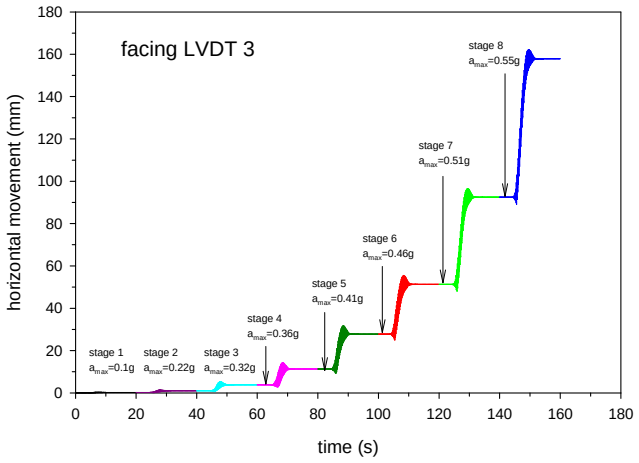

Fig. 6. Horizontal movement recorded by facing LVDT 3

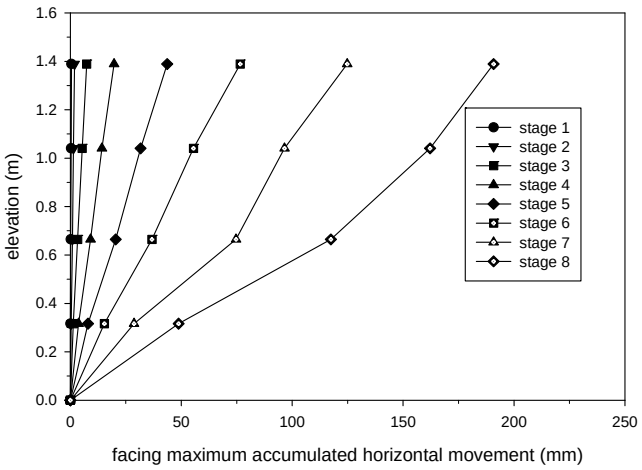

Fig. 7. Total maximum facing movement

trend was the accelerometer placed closest to the backfill surface which showed a generally decreasing trend after stage 4 shaking. Figure 9 presents the results of typical FFT analysis for one accelerometer at the third stage of shaking. The results for all accelerometers showed that the predominant frequency of excitation at all locations was equal to the target excitation value of 5 Hz. In order to investigate acceleration amplification, two different approaches were adopted here. The first method uses the ratio computed as the maximum measured acceleration at each accelerometer location divided by the maximum input base acceleration measured by the shaking table accelerometer (Fig. 10a). The second method uses the ratio of the maximum Fast Fourier Transform (FFT) of each measured acceleration record and the maximum FFT magnitude of the shaking table accelerometer (Fig. 10b).

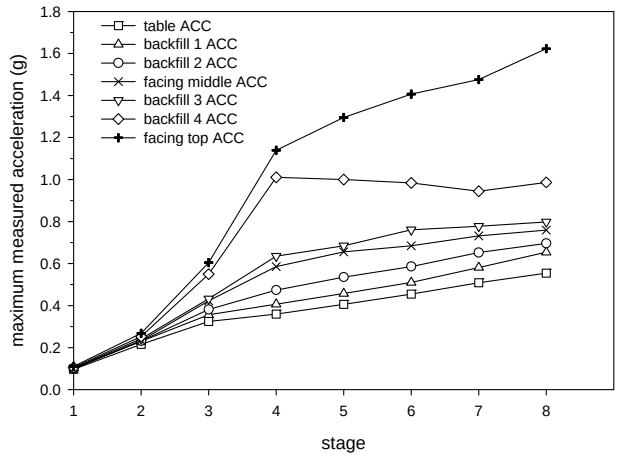

Fig. 8. Maximum measures acceleration

Both sets of results show that there is significant acceleration amplification along the facing panel height and inside the backfill soil. The maximum acceleration amplification factor at the top of the facing panel is about 3.25 and 2.7 measured by the acceleration ratio method and FFT ratio method, respectively. The maximum acceleration amplification in the backfill soil measured by the top accelerometer at the backfill surface is about 2.8 and 2 based on acceleration ratio method and FFT ratio method, respectively. The results also show that up to stage 4 the acceleration amplification factor calculated by both methods increased as the input base acceleration was increased. After stage 4 shaking however, only the bottommost backfill accelerometer showed a small increase in amplification factor while all other accelerometers show a decreasing trend in amplification factor as the base input acceleration increases. The decreasing trend in amplification factor is most pronounced for the accelerometers located at the top of the backfill and at the top of the facing panel. This is attributed to the proximity of the top free boundary and relatively low soil confinement at the top of the backfill allowing relatively large cyclic shear movements to occur.

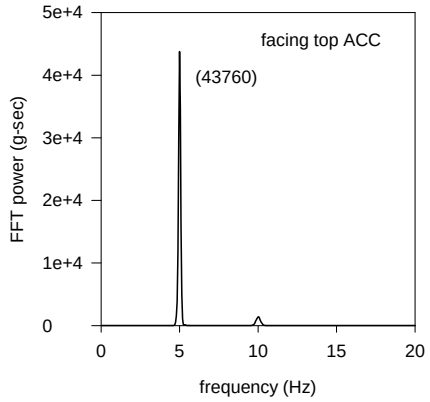

Fig. 9. FFT analysis of accelerometer response at stage 3 of shaking

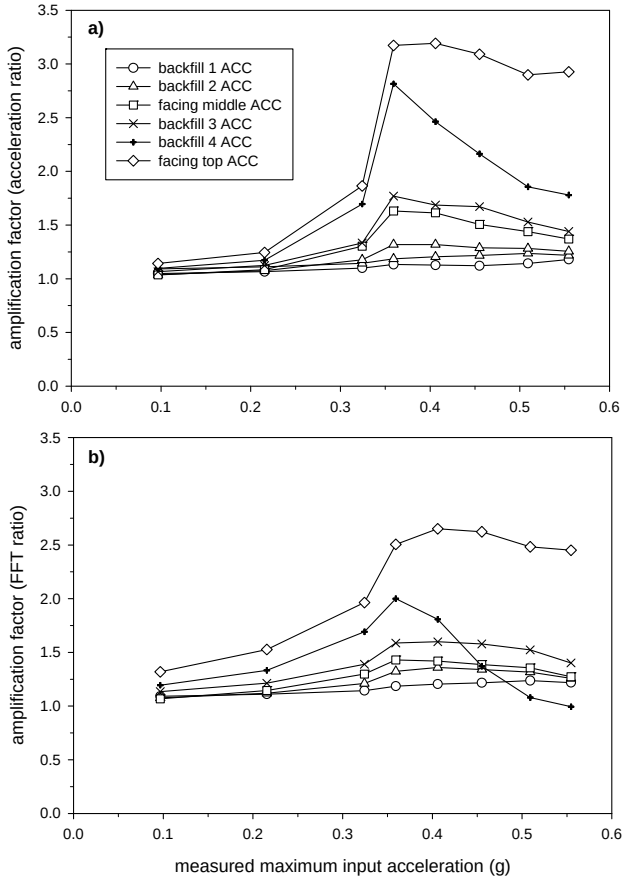

Fig. 10. Acceleration amplification factor calculated by: a) acceleration ratio, b) FFT ratio

Figure 11 illustrates data taken over the 0.14-second time interval corresponding to peak excitation during stage 4 shaking. Time delays between peak values of acceleration response are evident. Time delays (phase difference) taken with respect to the time of peak base excitation are shown in Fig. 12. Out-of-phase response is judged to occur only after stage 3 shaking. The maximum time delay in the backfill accelerometers occurs in the top accelerometer located close to the backfill top surface during stage 8 and is about 0.055 seconds. Based on the calculated time delays and the vertical distance between the backfill accelerometers, the shear wave velocity of the backfill soil is computed to be in the range of 142 and 26 m/s. Assuming a constant density of backfill soil during shaking, these shear wave velocities correspond to shear modulus values ranging between 34 and 2 MPa depending on elevations and shaking stages. These values fall within the range of shear wave velocities reported in the literature (Ishihara, 1996).

Strain gauges

Maximum tensile strains measured by the strain gauges attached to the longitudinal members of the geogrid are presented in Fig. 13 for all five layers of geogrid at each stage

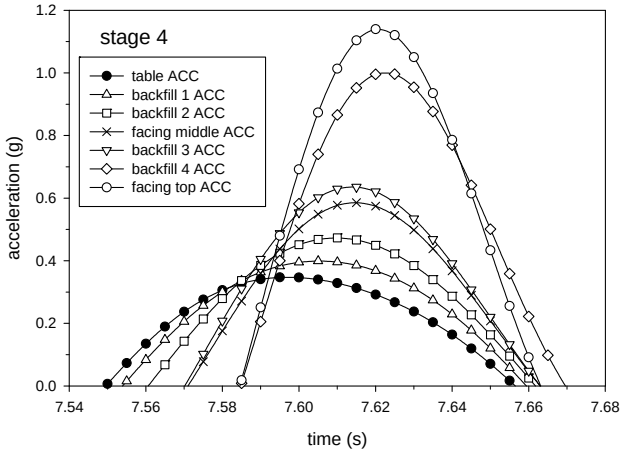

Fig. 11. Acceleration response during 0.14-second at peak excitation

of shaking. In general, the strain in each plot in each figure is time coincident. The results show that the highest tensile strain occurred in the bottom geogrid layer. Generally, as the shaking magnitude was increased, the tensile strains in all geogrid layers also increased. The smallest tensile strains occurred in the topmost geogrid layer due to the relatively low soil confinement.

Connection load rings

Figure 14 presents peak geogrid tensile loads measured by the connection load rings. The results illustrate that the maximum tensile loads generally increased with depth below the wall crest which is consistent with strain gauge measurements. There is a significant increase in geogrid tensile loads after stage 4 shaking (peak acceleration = 0.36 g). This is consistent with threshold response increases for facing deformations and acceleration magnitude reported earlier. The magnitude of acceleration threshold to generate this jump in wall response measurements is similar to the results of GRS shaking table tests with 1-m high wall models reported by El Emam and Bathurst (2004).

Vertical toe load cells

Vertical loads at the wall footing were measured by eight load cells supporting the base plate at the toe of the wall. The maximum values of the sum of vertical load cell readings are plotted in Fig. 15. The dashed line in the figure demonstrates that under static loading conditions the vertical loads at the footing are higher than the facing self-weight. This is attributed to additional soil down drag forces at the reinforcement layer connections due to soil compaction during construction and soil settlement when the wall facing moves out at initial prop release. This mechanism has been observed

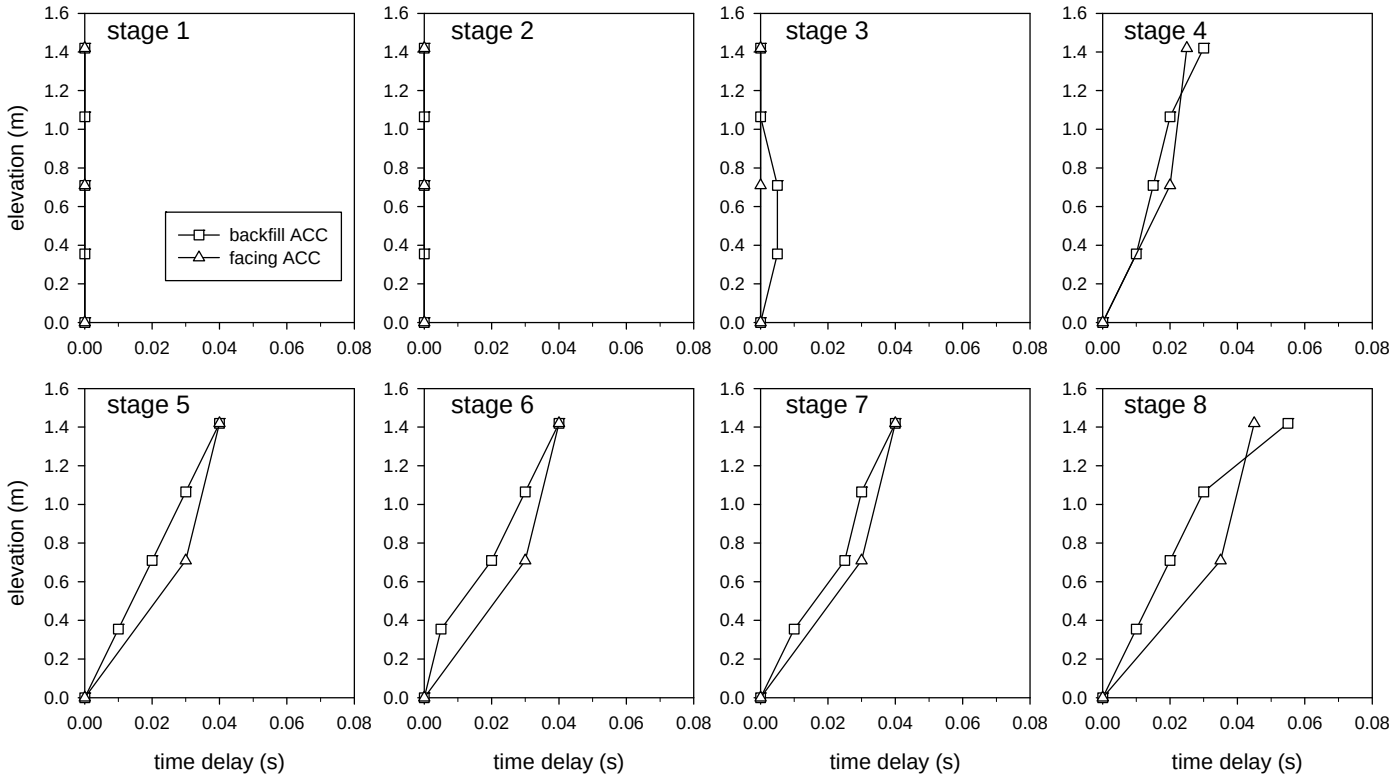

Fig. 12. Time delays at peak base input acceleration

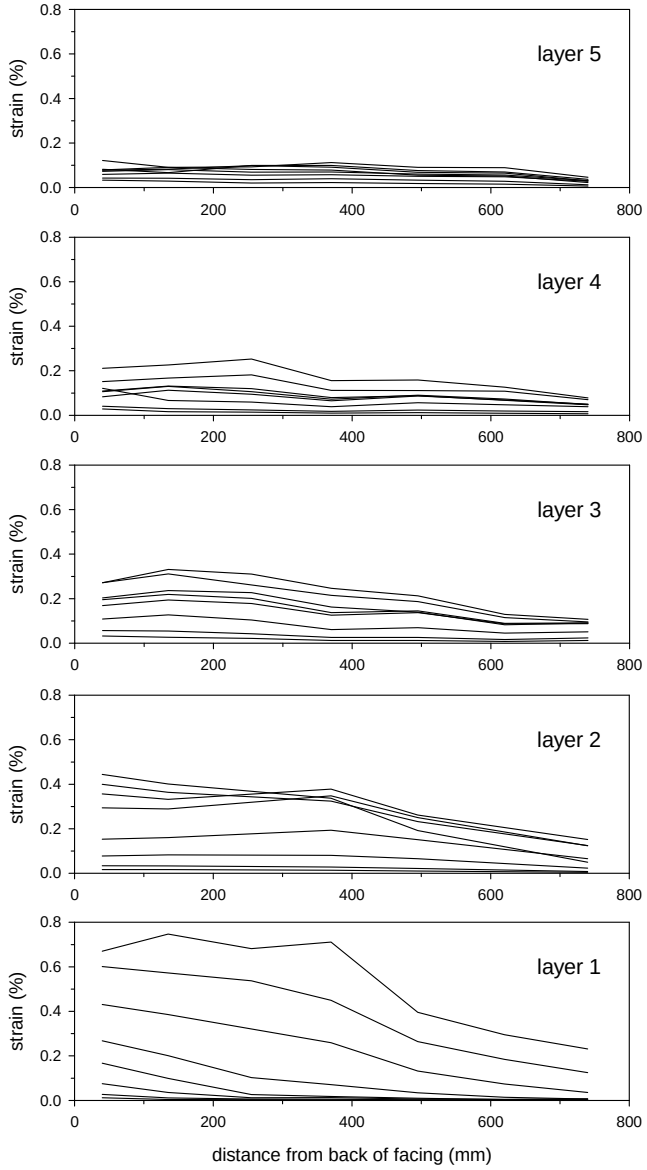

Fig. 13. Maximum strain values measured by geogrid strain gauges

in both reduced- and full-scale GRS wall models (El Emam and Bathurst 2004, Bathurst et al. 2001). Superimposed on the figures is the predicted total vertical toe load (facing self-weight plus down drag force) using Mononobe-Okabe wedge theory assuming that the wall-soil interface friction angle is 48 degrees and using the peak acceleration value at the base of the model. There is good agreement between the predicted and measured values.

Particle Image Velocimetry (PIV)

PIV analysis was used to track sand movements and facing panel movements. The field of view (Fig. 1) covered about 18 facing panels (out of 20) and most of the reinforced backfill zone. The ends of the facing hollow steel sections were tracked by PIV analysis at each shaking stage. The results of

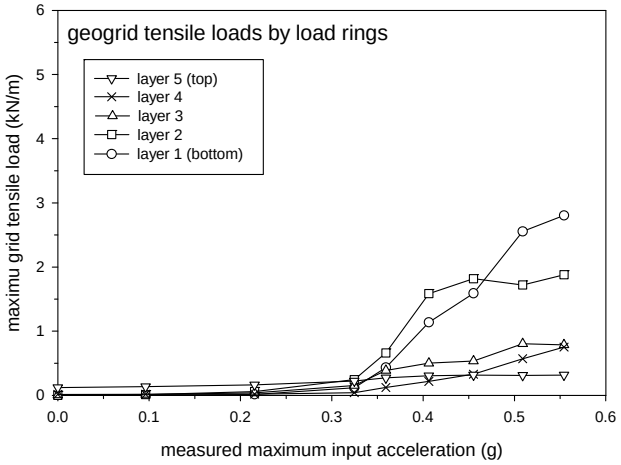

Fig. 14. Grid tensile loads at the connection to the facing

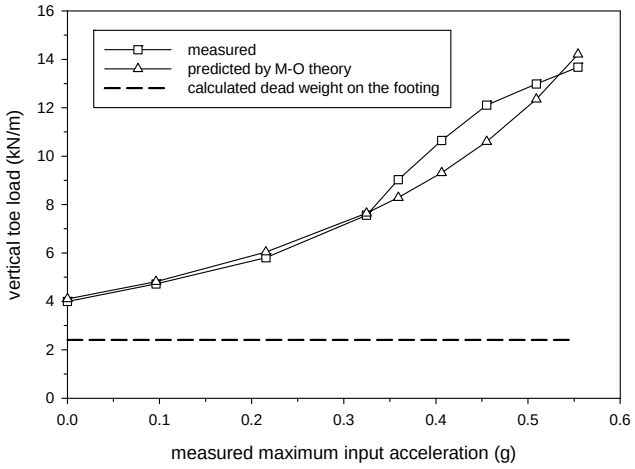

Fig. 15. Vertical toe loads at the wall footing

PIV analysis of incremental facing panel horizontal outward movement are presented in Fig. 16. The facing movements measured by the LDVTs are also plotted. It should be added that the PIV analysis for stages 7 and 8 could not be performed because sections of the facing moved out of the field of view, shadows appeared, or there was loss of texture in the images. These are lessons learned for future tests. Nevertheless, where there are PIV data there is good agreement between PIV results and LVDT measurements.

The backfill movement was also tracked by PIV analysis with 199 patches. Figure 17 shows vector plots of backfill movement measured at different times during the same peak excitation cycle during stage 4. The datum for each plot is the image taken at the start of stage 4 excitation when wall acceleration is zero. The end point in Fig. 17a corresponds to the peak displacement in the excitation cycle (positive or outward direction) and Fig. 17e corresponds to the minimum point in the excitation cycle (negative or inward direction). The vector magnitudes are amplified 15 times for clarity. As shown in Fig. 17a, the backfill outward movement is

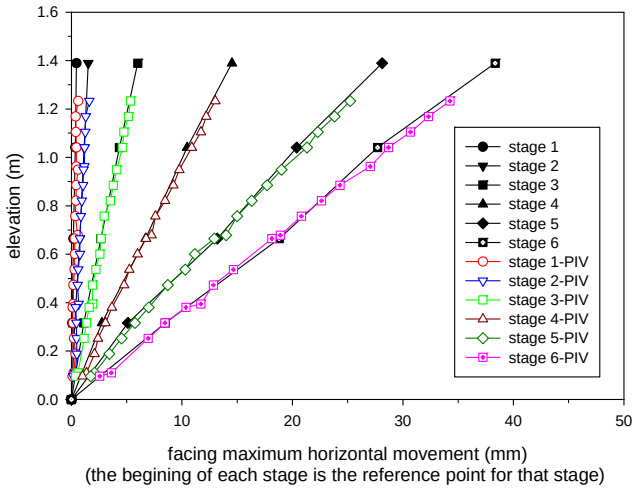

Fig. 16. Facing movement recorded during each shaking stage using PIV analysis and LVDTs

maximum and the pattern of vectors clearly shows this outward movement. Figure 17c corresponds to a middle point in the excitation cycle. There is no significant movement in the lower portions of the backfill and the movement over the top of the field of view is smaller than in Fig. 17a. In Fig. 17d the shaking table is moving in the negative direction (backward) and the vector plots show this movement at the bottom of the backfill. It is interesting to note that there is a detectable reversal in direction of movement in the top portion of the backfill soil and there is a diagonal band in the backfill that separates zones of positive and negative movement. In Fig. 17e the maximum shaking table movement is in the negative direction and is visible by the vectors at the lower part of the backfill. However, there is a change in movement direction occurring closer to the top of the backfill soil.

This observation is consistent with phase differences observations described earlier. However, the PIV-generated vector plots demonstrate the potential of the PIV method to qualitatively and quantitatively identify displacement mechanisms at small temporal and spatial scales.

Figures 18a and 18b show contour plots of total displacement during stage 4 at the peak input acceleration and at the end of the stage, respectively. The contours of maximum displacement in Fig. 18a range between 3.3 and 12.2 mm and

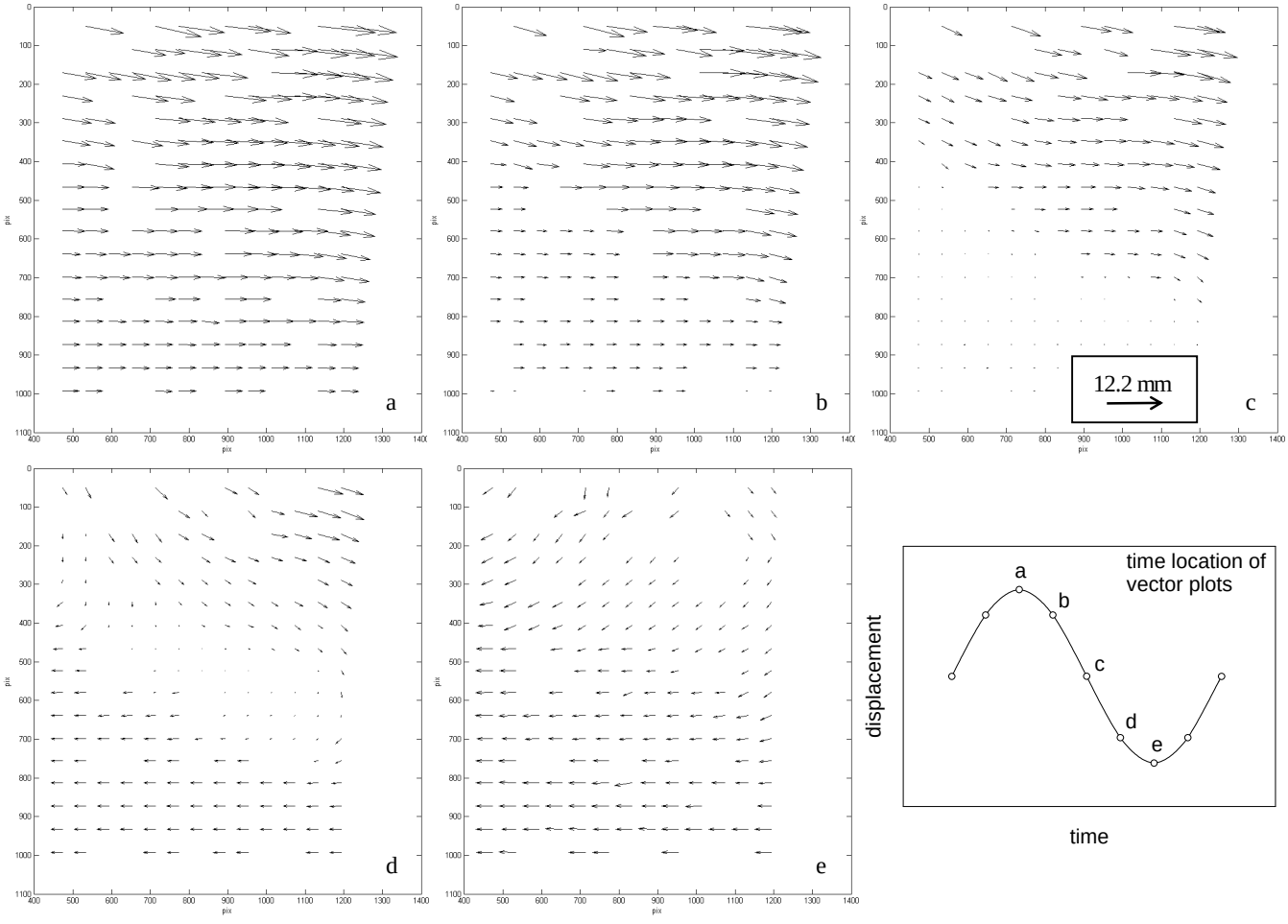

Fig. 17. Displacement vector plots at peak acceleration cycle at stage 4 (15 times enlarged), maximum = 12.2 mm

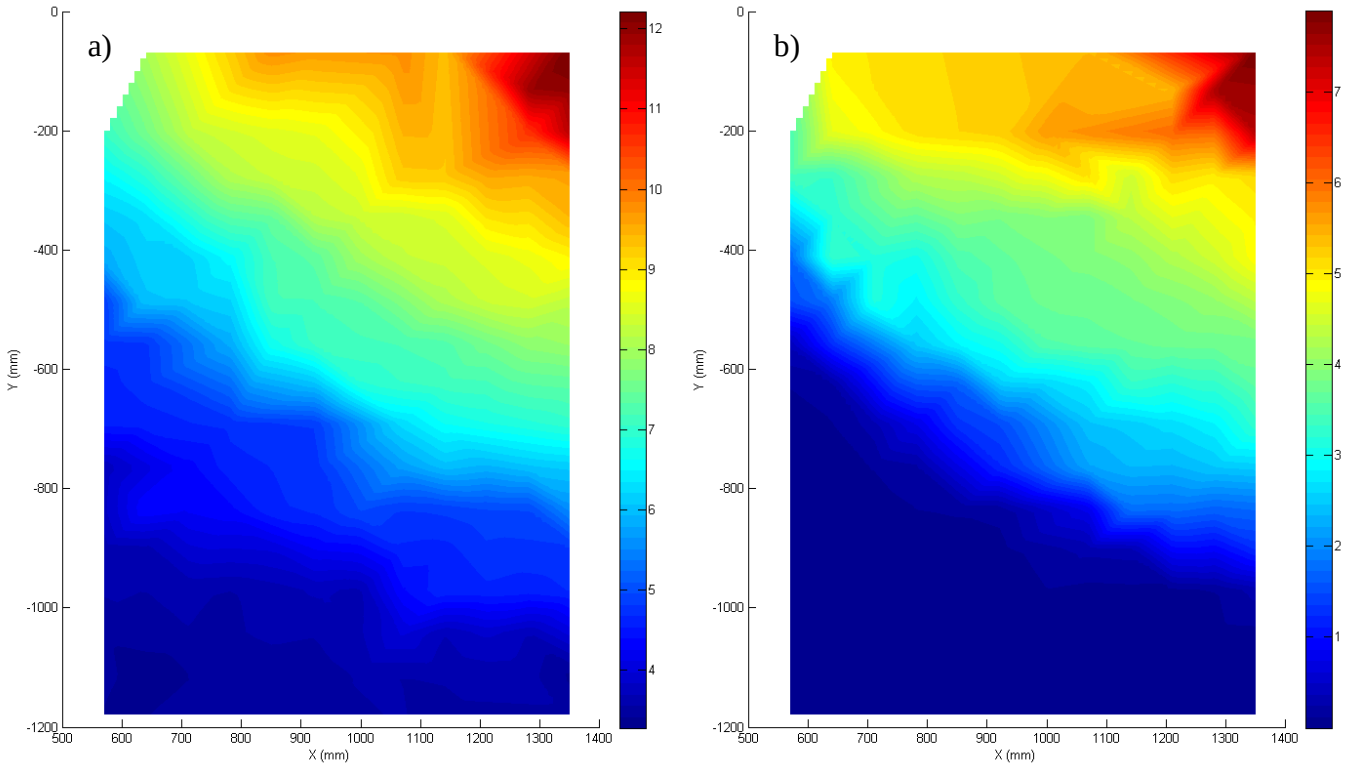

Fig. 18. Contours of: a) peak total displacement during stage 4 (3.3 to 12.2 mm); b) final total displacement at the end of stage 4 (0 to 7.9 mm)

the contours of residual displacement in Fig. 18b range between 0 to 7.9 mm. These displacements were calculated with respect to the initial image at the beginning of stage 4 as noted earlier. The plots clearly show the increase in peak and residual total displacement in the backfill soil as it gets closer to the surface of the backfill and close to the facing panels. It also shows the pattern of backfill soil movement and development of slip planes in the backfill due to base excitation.

CONCLUSIONS

This paper has focused on details of the experimental design, instrumentation and data interpretation that was developed as part of an ongoing investigation of the dynamic response of GRS walls using a large shaking table. The test set-up is unique because of the wide array of instrumentation that is deployed in each test. Of special interest is the use of the PIV method to measure sand backfill and facing displacements. The PIV method in combination with high speed camera imagery can be used to gather quantitative data at fine temporal and spatial scales which is useful to identify mechanisms and to verify analytical and numerical models.

REFERENCES

Allen, T.M. and R.J. Bathurst. [2002]. “Soil Reinforcement Loads in Geosynthetic Walls at Working Stress Conditions”, Geosynthetics International, Vol. 9, Nos. 5&6, pp. 525-566.

Bathurst, R.J., Z. Cai, and M.J. Pelletier. [1996]. “Seismic Design and Performance of Geosynthetic Reinforced Segmental Retaining Walls”, *Proc. of 10th annual Symp. of the Vancouver Geotechnical Society*, Vancouver, BC, 26 p.

Bathurst, R.J. and K. Hatami. [1998]. “Seismic Response Analysis of a Geosynthetic Reinforced Soil Retaining Wall”, Geosynthetics International, Vol. 5, Nos. 1&2, pp. 127-166

Bathurst, R.J., D.L. Walters, K. Hatami and T.M. Allen. [2001]. “Full-Scale Performance Testing and Numerical Modeling of Reinforced Soil Retaining Walls”, *International Symposium on Earth Reinforcement, IS Kyushu 2001*, Fukuoka, Japan, Vol. 2, pp. 777-799.

Bathurst, R.J., K. Hatami and M.C. Alfaro. [2002]. “Geosynthetic Reinforced Soil Walls and Slopes: Seismic Aspects”. In *Geosynthetics and Their Applications* (S.K. Shukla Ed.), Thomas Telford, pp. 327-392.

Collin, J.G., V.E. Chouery-Curtis, R.R. Berg. [1992]. “Field Observations of Reinforced Soil Structures under Seismic Loading”, *Proc. Int. Symp. Earth Reinforcement*, pp. 223–228.

El-Emam, M. and R.J. Bathurst. [2004]. "Experimental Design, Instrumentation and Interpretation of Reinforced Soil Wall Response Using a Shaking Table", International Journal of Physical Modeling in Geotechnics, Vol. 4, pp. 13–32.

El-Emam, M. and R.J. Bathurst. [2005]. "Facing Contribution to Seismic Response of Reduced-Scale Reinforced Soil Walls", Geosynthetics International, Vol. 12, No. 3, pp. 215–238.

Hatami, K. and R.J. Bathurst. [2005]. "Development and Verification of a Numerical Model for the Analysis of Geosynthetic Reinforced Soil Segmental Walls under Working Stress Conditions", Canadian Geotechnical Journal, Vol. 42, No. 4, pp. 1066-1085.

Hatami, K., R.J. Bathurst, and P. Di Pietro. [2001]. "Static Response of Reinforced Soil Retaining Walls with Non-Uniform Reinforcement", International Journal of Geomechanics, Vol. 1, No.4, pp. 477-506.

Iai, S. [1989]. "Similitude for Shaking Table Tests on Soil-Structure-Fluid Model in 1g Gravitational Field", Soils and Foundations, 29, No. 1, pp. 105–118.

Ishihara, K. [1996]. "*Soil Behavior in Earthquake Geotechnics*". Clarendon Press, Oxford.

Kato, N., C.C. Huang, M. Tateyama, K. Watanabe, J. Koseki and F. Tatsuoka. [2002]. "Seismic Stability of Several Types of Retaining Walls on Sand Slope", *Proc. of 7th Int. Conf. on Geosynthetics*, Nice, Italy, pp. 237-240.

Koseki, J., Y. Munaf, F. Tatsuoka, M. Tateyama, K. Kojima and T. Sato. [1998]. "Shaking and Tilt Table Tests of Geosynthetic-Reinforced Soil and Conventional-Type Retaining Walls", Geosynthetics International, Vol. 5, Nos. 1&2, pp. 73-96.

Koseki, J., R.J. Bathurst, E. Güler, J. Kuwano and M. Maugeri. [2006]. "Seismic Stability of Reinforced Soil Walls", Invited keynote paper, *8th Int. Conf. on Geosynthetics*, Yokohama, Japan, 30 p.

Ling, H.I., D. Leshchinsky and N.N.S. Chou. [2001]. "Post-Earthquake Investigation on Several Geosynthetic-Reinforced Soil Retaining Walls and Slopes During 1999 Ji-Ji Earthquake of Taiwan", Soil Dynamics and Earthquake Engineering, Vol. 21, No. 4, pp. 297–313.

Ling, H.I., Y. Mohri, D. Leshchinsky, C. Burke, K. Matsushima and H. Liu. [2005]. "Large-Scale Shaking Table Tests on Modular-Block Reinforced Soil Retaining Walls", Journal of Geotechnical and Geoenvironmental Engineering, ASCE, Vol. 131, No. 4, pp. 465-476.

Lo Grasso, A.S., M. Maugeri and P. Recalcati. [2004]. "Response Of Geosynthetic Reinforced Soil Wall Under Seismic Condition by Shaking Table Tests", *3rd European Geosynthetics Conf.*, Munich, Germany, 6 p.

Matsuo, O., T. Tsutsumi, K. Yokoyama and Y. Saito. [1998]. "Shaking Table Tests and Analyses of Geosynthetic-Reinforced Soil Retaining Walls", Geosynthetics International, Vol. 5, No. 1&2, pp. 97-126.

NCMA, [1998]. "*Design Manual for Segmental Retaining Walls*". 2nd edn (ed. J. Collin). Herdon, VA: National Concrete Masonry Association.

Rowe, R.K. and S.K. Ho. [1998]. "Horizontal Deformation in Reinforced Soil Walls", Canadian Geotechnical Journal, Vol. 35, No. 2, pp. 312-327.

Sakaguchi, M. [1996]. "A Study of the Seismic Behavior of Geosynthetic Reinforced Walls in Japan", Geosynthetics International, Vol. 3, No. 1, pp. 13-30.

Sandri, D. [1997]. "A Performance Summary of Reinforced Soil Structures in the Greater Los Angeles Area after the Northridge Earthquake", Geotextiles and Geomembranes, Vol. 15, pp. 235-253.

Tatsuoka, F., M. Tateyama and J. Koseki. [1995]. "Behavior of Geogrid-Reinforced Soil Retaining Walls during the Great Hanshin-Awaji Earthquake", *Proc. 1st Int. Symp. Earthquake Geotechnical Eng.*, Vol. 2, pp. 55–60.

Tatsuoka, F., M. Tateyama, T. Uchimura and J. Koseki. [1997a]. "Geosynthetic-Reinforced Soil Retaining Walls as Important Permanent Structures", Geosynthetics International, Vol. 4, No. 2, pp. 81-136.

Tatsuoka, F., J. Koseki and M. Tateyama. [1997b]. "Performance of Reinforced Soil Structures during the 1995 Hyogo-Ken Nanbu Earthquake", Earth Reinforcement, Balkema, Vol. 2, pp. 973- 1008.

Watanabe, K., Y. Munaf, J. Koseki, M. Tateyama and K. Kojima. [2003]. "Behaviors of Several Types of Model Retaining Walls Subjected to Irregular Excitation", Soils and Foundations, Vol. 43, No. 5, pp. 13-27.

White, D. and R.D. Holtz. [1997]. "Performance of Geosynthetic Reinforced Slopes and Walls during the Northridge California Earthquake of Jan. 17, 1994", Ochiai, H., Yasufuku, N., Omine, K. (Eds.), Earth Reinf., Balkema, Rotterdam, pp. 965–972.

White, D.J., W.A. Take and M.D. Bolton. [2003]. "Soil Deformation Measurement Using Particle Image Velocimetry (PIV) and Photogrammetry", Geotechnique, Vol. 53, No. 7, pp. 619-631.